

Evaluation of Self-generated Behavior: Untangling Metacognitive Readout and Error Detection

Tadeusz W. Kononowicz and Virginie van Wassenhove

Abstract

■ When producing a duration, for instance, by pressing a key for 1 sec, the brain relies on self-generated neuronal dynamics to monitor the “flow of time.” Evidence has suggested that the brain can also monitor itself monitoring time, the so-called self-evaluation. How are temporal errors inferred on the basis of purely internally driven brain dynamics with no external reference for time? Although studies have shown that participants can reliably detect temporal errors when generating a duration, the neural bases underlying the evaluation of this self-generated temporal behavior are unknown. Theories of psychological time have also remained silent about such self-evaluation abilities. We assessed the contributions of an error-detection mechanism, in which error detection results from the ability to estimate the latency of motor actions, and of a readout

mechanism, in which errors would result from inferring the state of a duration representation. Error detection predicts a V-shape association between neural activity and self-evaluation at the offset of a produced interval, whereas the readout predicts a linear association. Here, human participants generated a time interval and evaluated the magnitude of their timing (first- and second-order behavioral judgments, respectively). Focusing on the MEG/EEG signatures after the termination of the self-generated duration, we found several cortical sources involved in performance monitoring displaying a linear association between the power of alpha ($\alpha = 8\text{--}14$ Hz) oscillations and self-evaluation. Altogether, our results support the readout hypothesis and indicate that duration representation may be integrated for the evaluation of self-generated behavior. ■

INTRODUCTION

Metacognition refers to the knowledge gained in introspecting one’s cognitive states (Fleming & Dolan, 2012; Flavell, 1979). Metacognition is often investigated through the evaluation of confidence on a perceptual decision task; thereby, a second-order decision (e.g., confidence rating) is contingent on a first-order judgment (e.g., discrimination of stimuli). Metacognition thus necessitates a meta-representation of the first-order judgment (Fleming, Dolan, & Frith, 2012). Here, we explored the meta-representation of endogenous timing, namely, whether the mechanisms by which the representation of a duration can serve temporal metacognition (TMC).

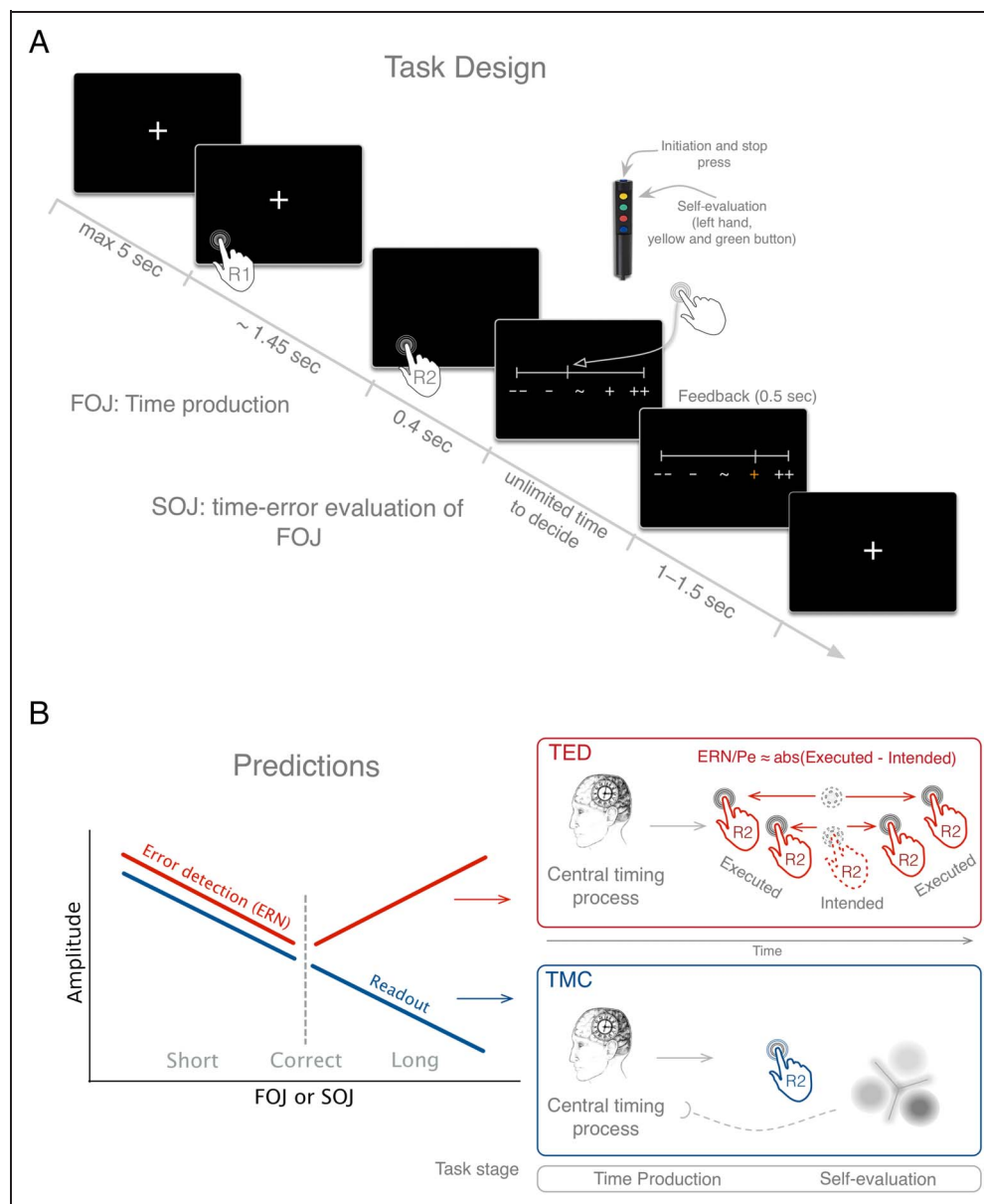
In a seminal study, human participants receiving incorrect feedback after their time production showed a negative evoked brain response (Miltner, Braun, & Coles, 1997; then coined error-related negativity [ERN], now corresponding to feedback-related negativity). The observed ERN was interpreted as reflecting the difference between participants’ internal belief about the correctness of their time production and the objective feedback. These observations suggested the internal representation

of an intended duration could be studied from the perspective of metacognition. Later empirical evidence across species further hinted at the notion of self-evaluation in timing: For instance, seminal work has shown that the combination of uncertainties of internal representations and external cues could serve temporal monitoring in both rats and humans (Balci, Freestone, & Gallistel, 2009). In a duration discrimination task, rats were described to decline the test more often when they were presented with uncertain stimuli (Foote & Crystal, 2007). More recently, humans were shown to reliably report their temporal errors after time reproduction (i.e., the motor reproduction of a sensory time interval; Akdoğan & Balci, 2017) and after their time production (i.e., the self-generation of a time interval in the absence of sensory template, Figure 1A; Kononowicz, Roger, & van Wassenhove, 2019). Altogether, these results suggest the availability of the accuracy and precision of temporal representation for TMC, yet existing theories of psychological time have remained silent about the possibility of introspecting or self-evaluating one’s internal time.

Here, we investigated the neural responses after time production and tested two hypothetical mechanisms, which could serve the representation of temporal errors during a time production task. First, in the currently investigated data set, we have recently showed that the dynamics of beta oscillatory activity ($\beta = 15\text{--}40$ Hz)

Cognitive Neuroimaging Unit, CEA DRF/Joliot, INSERM, Université Paris-Sud, Université Paris-Saclay, NeuroSpin Center, 91191 Gif/Yvette, France

Figure 1. Experimental paradigm and predictions. (A) Time course of one experimental trial. (B) Predictions of the TED (red) and temporal metacognitive readout (TMC; blue) working hypotheses. According to TED, the evaluation of a temporal error arises from the timing difference between the intended latency of motor action execution (dashed hand as the expected latency of the motor plan) and the actual executed action (solid hand happening anytime before or after the intended action). This temporal residual error would be captured by the variability of the ERN/Pe amplitude [$ERN/Pe \approx \text{abs}(\text{Executed} - \text{Intended})$]; The further away from the intended latency, the larger the ERN/Pe irrespective of whether the act occurred earlier or later than intended. In the alternative TMC hypothesis, the evaluation of the temporal residual error relies on a metarepresentation of duration. Contrary to the TED hypothesis, the TMC hypothesis proposes the internal representation of duration and a readout mechanism that would actively infer the state of this internal timing variable. The TMC would elicit sustained components, and a signature of the readout would show a linear scaling of the neural response with the produced duration after the temporal production (blue line).



during time production predicted the accuracy of both the self-generated time intervals and their self-evaluation (Kononowicz et al., 2019). The observation of a common cortical signature for first- and second-order temporal estimates suggested that β power may instantiate the intended duration (first-order estimate) and serve as a readable variable for second-order estimation. In other words, we formulated the TMC hypothesis, which posits the existence of an internal representation of duration as a β state-dependent network and a readout mechanism, which would actively infer the state of this internal timing variable (Grabot et al., 2019). A temporal metacognitive readout was predicted to linearly code for the state of the networks coding the duration at the outset of the timed interval (Laje & Buonomano, 2013; Simen, Balci, de Souza, Cohen, & Holmes, 2011; Ivry & Schlerf, 2008; Karmarkar & Buonomano, 2007). In this study,

we thus hypothesize that a neural signature of an internal duration readout would linearly scale with the produced duration after the production of a temporal interval (post-R2). We could not legitimately predict the sign of the linear scaling, and whether the amplitude of the readout signal would increase or decrease with increasingly produced duration could not be determined a priori.

Under the more classic temporal error detection (TED) hypothesis, temporal error monitoring would rely on the monitoring of motor actions with no specific need for a metarepresentation of duration. The TED hypothesis entails the estimation of a delay between the internally generated “go” signal and the latency of the actually executed action. For instance, using a simple RT task, Marti, Sackur, Sigman, and Dehaene (2010) asked participants to estimate the latency of their RTs on a trial-by-trial basis. Participants accurately estimated the latencies of their

motor actions. In line with TED, participants' ability to monitor the timing of their RTs could mediate temporal error monitoring during a timing task. The self-evaluation of "too short" productions could be supported by error-detection mechanisms because of premature responding, which is known to generate large error responses during EEG recordings (Scheffers & Coles, 2000). Similarly, the brain error responses were previously reported by Luu, Flaisch, and Tucker (2000), who investigated the neural correlates of monitoring the latency of executed actions: In their study, participants performed an RT task with a deadline response set to the median RT estimated during a practice block. The feedback could indicate that the response was on time or too late. Motor responses that occurred later than the response deadline elicited larger ERNs than those occurring earlier. Moreover, the ERN amplitude increased with increasing response delays, suggesting a temporal monitoring of the action latency (Luu et al., 2000). According to TED, the monitoring of motor action latency could serve temporal error monitoring and, by analogy to the estimation of the RT delays (Luu et al., 2000), would likely occur after the termination of the temporal production (R2). On this basis, we predicted the elicitation of an ERN (Cohen, 2014; Gehring, Goss, Coles, Meyer, & Donchin, 1993) when temporal production was off target. This working hypothesis was further supported by sensorimotor synchronization tasks in which the ERN amplitude was found to increase with temporal errors irrespective of their being early or late (Jantzen, Ratcliff, & Jantzen, 2018). Following the TED hypothesis, a V-shaped pattern was thus predicted so that the further away time productions were from the target, the larger the amplitude of the ERN (Figure 1B). Furthermore, as participants were capable of TMC in this task (Kononowicz et al., 2019), we predicted the elicitation of a Pe, an evoked response after the ERN, which has typically been reported to index the conscious evaluation of errors (Nieuwenhuis, Ridderinkhof, Blom, Band, & Kok, 2001; Falkenstein, Hohnsbein, Hoormann, & Bланке, 1991) and which takes into account proprioceptive and reafferent information (Nieuwenhuis et al., 2001).

In summary, the TED hypothesis relies on the online estimation of a motor action, whereas the TMC reads out the representation of duration. These two working hypotheses propose distinct anatomical and dynamical loci of temporal error monitoring in a time production task. Here, we investigated the neural mechanisms underlying temporal evaluation with two main working hypotheses: (i) TED of motor actions (Meckler et al., 2010; Praamstra, Turgeon, Hesse, Wing, & Perryer, 2003) and (ii) readout of an internal variable coding for duration (Figure 1B). For this, we quantified evoked and oscillatory brain activity locked to the offset of the produced time interval. We show how brain activity traces the self-evaluation of temporal production on a single-trial basis and describe a link between offset responses and timing signatures (β activity).

METHODS

Participants

Nineteen right-handed volunteers (11 women, mean age = 24 years) with no self-reported hearing/vision loss or neurological pathology were recruited for the experiment and received monetary compensation for their participation. Before the experiment, each participant provided a written informed consent in accordance with the Declaration of Helsinki (2008) and the Ethics Committee on Human Research at Neurospin (Gif-sur-Yvette). The data of seven participants were excluded from the analysis because of the absence of anatomical MRI (aMRI), technical issues with the head positioning system during MEG acquisition, abnormal artifacts during MEG recordings, and two participants not having finished the experiment. These data sets were excluded a priori and were neither visualized nor inspected. Thus, the final sample was composed of 12 participants (seven women, mean age = 24 years). All participants performed six experimental blocks. One block was removed for two participants because of excessive artifacts or lack of conformity to task requirements.

Stimuli and Procedure

Before the MEG acquisitions, it was explained to participants that they were taking part in a time estimation experiment, and written instructions were provided explaining all steps of the experimental protocol. In each trial, participants were first asked to produce a 1.45-sec time interval and then to rate whether their production was shorter or longer than the target interval on a linear scale. After each rating, they received feedback on their time production (not on their self-evaluation; Figure 1A). We will refer to the produced time interval as the first-order temporal judgment (FOJ) and to the self-evaluation of the first-order judgment as the second-order temporal judgment (SOJ).

Each trial started with the presentation of a fixation cross "+" on the screen indicating that participants could start whenever they decided to (Figure 1A). The intertrial interval ranged between 1 and 1.5 sec. Participants initiated their time production with a brief but strong button press once they felt relaxed and ready to start. Once they estimated that a 1.45-sec interval had elapsed, they terminated the interval by another brief button press. To initiate and terminate their time production (FOJ), participants were asked to press the top button of a Fiber Optic Response Pad (FORP; Science Plus Group) using their right thumb (Figure 1A). The "+" was removed from the screen during the estimation of the time interval to avoid any sensory cue or confounding responses in brain activity related to the FOJ.

After the production of the time interval, participants were asked to self-evaluate their time estimation (second-order judgment; Figure 1A). For this, participants were

provided with a scale displayed on the screen 0.4 sec after the keypress that terminated the produced time interval. Participants could move a cursor continuously using the yellow and green FORP buttons (Figure 1A). Participants were instructed to place the cursor according to how close they thought their FOJ was with respect to the instructed target interval indicated by the sign “~” placed in the middle of the scale. Participants placed the cursor to indicate whether they considered their produced time interval to be too short (“- -,” left side of the scale) or too long (“+ +,” right side of the scale). Participants could take as much time as needed to be accurate in their SOJ.

After the completion of the SOJ, participants received feedback displayed on a scale identical to the one used for SOJ. Participants received feedback on all trials in the first and fourth experimental blocks and on 15% of the trials in all other blocks (Figure 1A). The row of five symbols indicated the length of the just-produced FOJ (Figure 1A). The feedback range was set to the value of the perceptual threshold estimated on a per-individual basis (mean population threshold = 0.223 sec, $SD = 0.111$ sec). A near-correct FOJ yielded the middle “~” symbol to turn green; a too short or too long FOJ turned the symbols “-“ or “+” orange, respectively (Figure 1A); and a FOJ that exceeded these categories turned the symbols “- -“ or “+ +” red. In Blocks 1 and 4, participants received feedback in all trials; in Blocks 2, 3, 5, and 6, participants received feedback in 15% of randomly selected trials. From Block 4 on, and unbeknownst to participants, the target duration was increased to 1.45 sec + individual threshold/2 (mean population duration = 1.56 sec). This experimental manipulation was outside the scope of this study and was tackled in another specific analysis showing the possibility of implicit temporal recalibration (cf. Kononowicz et al., 2019). On average, the new target duration was 1.56 sec based on the average threshold. All six blocks were used in the subsequent analyses.

In Blocks 1 and 4, participants had to produce 100 trials; in Blocks 2, 3, 5, and 6, participants produced 118 trials. Between the experimental blocks, participants were reminded to produce the target duration of 1.45 sec as accurately as possible and to maximize the number of correct trials in each block.

Estimation of Temporal Discrimination Thresholds

The Psychoacoustics toolbox was used to calculate the temporal discrimination threshold for each participant (Soranzo & Grassi, 2014) by adapting the available routine “DurationDiscriminationPureTone” provided in the toolbox. An adaptive procedure was chosen using a staircase method with a two-down one-up rule and stopped after 12 reversals (Levitt, 1971). For each trial, three identical tones of 1 kHz were presented to the participants. One of the tones lasted longer than 1.45 sec (deviant

tone), whereas the other two tones lasted precisely 1.45 sec (standard tones). The position of the deviant tone changed randomly across trials. The task was to identify the deviant tone and to give its position in the sequence. Tones were provided by earphones binaurally. The value of the correct category was set as target duration \pm (threshold/3), and the lower and upper limits were set as target duration \pm ($2 \times$ individual threshold/3), respectively. These values were used to provide feedback to participants. Although this method did not provide a direct assessment of an individual’s temporal production discrimination threshold, the link between auditory and motor timing has been noted (e.g., Meegan, Aslin, & Jacobs, 2000) and is considered functionally relevant (e.g., Zatorre, Chen, & Penhune, 2007).

Simultaneous MEG/EEG Recordings

The experiment was conducted in a dimly lit, standard magnetically shielded room located at Neurospin (CEA/DRF) in Gif-sur-Yvette. Participants sat in an armchair with eyes open looking at a screen used to show visual stimuli using a projector located outside the magnetically shielded room. Participants were asked to respond by pushing a button on a FORP response pad held in their right hand. Electromagnetic brain activity was recorded using the whole-head Elekta Neuromag Vector View 306 MEG system (Neuromag Elekta Ltd.) equipped with 102 triple-sensor elements (two orthogonal planar gradiometers and one magnetometer per sensor location) and the 64 native EEG system using Ag–AgCl electrodes (EasyCap) with impedances below 15 k Ω . Participants sat in an upright position. Their head position in the dewar was measured before each block using four head-position coils placed over the frontal and mastoid areas. The four head-position coils and three additional fiducial points (nasion, left and right preauricular areas) were digitized for subsequent coregistration with the individual’s aMRI. MEG and EEG (M/EEG) recordings were sampled at 1 kHz and band-pass filtered between 0.03 and 330 Hz. The EOGs (horizontal and vertical eye movements), electrocardiograms, and electromyographics were recorded simultaneously with MEG. The head position with respect to the MEG sensors was measured using coils attached to the scalp. The locations of the coils and EEG electrodes were digitized with respect to three anatomical landmarks using a 3-D digitizer (Polhemus). Stimuli were presented using a PC running Psychtoolbox software (Brainard, 1997) that has been executed in MATLAB environment.

DATA ANALYSIS

M/EEG Data Preprocessing

Signal space separation correction (Taulu & Simola, 2006), head movement compensation, and bad channel rejection were done using MaxFilter Software (Elekta

Neuromag). Trials containing excessive ocular artifacts, movement artifacts, amplifier saturation, or SQUID artifacts were automatically rejected using rejection criterion applied on magnetometers ($55e^{-12}$ T/m) and on EEG channels ($250e^{-6}$ V). Trial rejection was performed using epochs ranging from -0.8 to 2.5 sec after the first press initiating the time production trial. Eye blinks, heartbeats, and muscle artifacts were corrected using independent component analysis (Bell & Sejnowski, 1995) with MNE-Python. Baseline correction was applied using the mean value ranging from -0.3 to -0.1 sec before the first keypress.

Preprocessed M/EEG data were analyzed using MNE-Python 0.13 (Gramfort et al., 2014) and custom-written Python code. For the analysis of evoked responses in the time domain, a low-pass zero-phase lag finite impulse response filter (40 Hz) was applied to raw M/EEG data. For time–frequency analyses, raw data were filtered using a double-pass bandpass finite impulse response filter (0.8–160 Hz). The high-pass cutoff was added to remove slow trends, which could lead to instabilities in time–frequency analyses. To reduce the dimensionality, all evoked and time–frequency analyses were performed on virtual sensor data combining magnetometers and gradiometers into single MEG sensor types using the *as_type* method from MNE-Python 0.13 for gradiometers. This procedure largely simplified visualization and statistical analysis without losing information provided by all types of MEG sensors (gradiometers and magnetometers).

M/EEG-aMRI Coregistration

aMRI was used to provide high-resolution structural images of each individual's brain. The aMRI was recorded using a 3-T Siemens Trio MRI scanner. Parameters of the sequence were as follows: voxel size = $1.0 \times 1.0 \times 1.1$ mm, acquisition time = 466 sec, repetition time = 2300 msec, and echo time = 2.98 msec. Volumetric segmentation of participants' aMRI and cortical surface reconstruction were performed with the FreeSurfer software (surfer.nmr.mgh.harvard.edu/). A multiecho FLASH pulse sequence with two flip angles (5° and 30°) was also acquired (Jovicich et al., 2006; Fischl et al., 2004) to improve coregistration between EEG and aMRI. These procedures were used for group analysis with the MNE suite software (Gramfort et al., 2014). The coregistration of the M/EEG data with the individual's structural MRI was carried out by realigning the digitized fiducial points with MRI slices. Using *mne_analyze* within the MNE suite, digitized fiducial points were aligned manually with the multimodal markers on the automatically extracted scalp of the participant. To ensure reliable coregistration, an iterative refinement procedure was used to realign all digitized points with the individual's scalp.

MEG Source Reconstruction

Individual forward solutions for all source locations located on the cortical sheet were computed using a three-layer boundary element model constrained by the individual's aMRI. Cortical surfaces extracted with FreeSurfer were subsampled to 10,242 equally spaced sources on each hemisphere (3.1 mm between sources). The noise covariance matrix for each individual was estimated from the baseline activity of all trials and all conditions. The forward solution, the noise covariance, and source covariance matrices were used to calculate the dynamic SPM estimates (Dale et al., 2000). The inverse computation was done using a loose orientation constraint (loose = 0.4, depth = 0.8) on the radial component of the signal. Individuals' current source estimates were registered on the FreeSurfer average brain for surface-based analysis and visualization.

ERF/ERP Analysis

The analyses of MEG evoked-related fields (ERFs) and EEG potentials (ERPs) focused on the quantification of the amplitude of slow evoked components using non-parametric cluster-based permutation tests, which control for multiple comparisons (Maris & Oostenveld, 2007). The critical cluster value used was 0.05. This analysis combined all sensors and electrodes into the analysis without predefining a particular subset of electrodes or sensors, thus keeping the set of M/EEG data as similar and consistent as possible. We used a period ranging from -0.3 to -0.1 sec before the first press as the baseline.

Time–Frequency Analysis

To analyze the oscillatory power in different frequency bands using cluster-based permutation, we used discrete prolate spheroidal sequence tapers with an adaptive time window of frequency/2 cycles per frequency in 4-msec steps for frequencies ranging from 3 to 100 Hz, using the *tfr_multitaper* function from MNE-Python. Time bandwidth for frequency smoothing was set to 2. To receive the desired frequency smoothing, the time bandwidth was divided by the time window defined by the number of cycles. For example, for 10-Hz frequency, time bandwidth was $2/0.5$, resulting in 4-Hz smoothing. We used -0.3 to -0.1 sec before the first press as the baseline. The statistical analyses performed on theta (3–7 Hz), alpha (8–14 Hz), β (15–40 Hz), and γ (41–100 Hz) bands used spatiotemporal cluster permutation tests in the same way as for evoked response analyses.

Cluster-Based Statistical Analysis of M/EEG Data

Cluster-based analyses identified significant clusters of neighboring electrodes or sensors in the millisecond

time dimension. To assess the differences between the experimental conditions as defined by behavioral outcomes, we ran cluster-based permutation analysis (Maris & Oostenveld, 2007), as implemented by MNE-Python by drawing 1,000 samples for the Monte Carlo approximation and using FieldTrip's default neighbor templates. The randomization method identified the MEG virtual sensors and the EEG electrodes whose statistics exceeded a critical value. Neighboring sensors exceeding the critical value were considered as belonging to a significant cluster. The cluster level statistic was defined as the sum of values of a given statistical test in a given cluster and was compared to a null distribution created by randomizing the data between conditions across multiple participants. The p value was estimated based on the proportion of the randomizations exceeding the observed maximum cluster-level test statistic. Only clusters with corrected $p < .05$ are reported. For visualization, we have chosen to plot the MEG sensor or the EEG electrode of the significant cluster, with the highest statistical power. For all performed analyses, we used the same window length (0.4 sec), unless stated otherwise in the Results section. We used the 0.4-sec window as it was the maximal window length that could be used post-R2, given the onset of visual stimulation 0.4 sec after the R2. There was no a priori reasons to change the window length in subsequent analyses, hence the same window length was kept for the analysis of oscillatory power before R2 and post-R1. The window length was only changed for single-trial analyses of evoked activity. The latencies of ERP components were selected at the predicted ERN and Pe latencies (see Relative contributions of evoked activity and α power to temporal error monitoring).

Behavioral Data Analysis

The analysis of behavioral data was performed using generalized additive mixed models (GAMMs; Wood, 2017), as fully described below in the Single-trial analysis section, unless stated otherwise in the Results section. Each model was fitted with participant as a random factor. For the analysis of metacognitive inference, SOJ was entered as a linear predictor of FOJ.

Binning Procedure of Behavioral and Neuroimaging Data

All cluster-based analyses were performed on three conditions defined on the basis of the objective performance in time production (FOJ: short, correct, long) or the subjective self-evaluation (SOJ: short, correct, long) separately for each experimental block. Before the binning, the behavioral data were z scored on a per-block basis to keep the trial count even in each category. Computing these three conditions within a block focused the analysis on local variations of brain activity as a function of objective or subjective performance. To overcome limitations

of arbitrary binning and to capitalize on the continuous performance naturally provided by the time production and the time self-evaluation tasks, we also used a single-trial approach, which investigated the interactions between the first- and second-order terms.

Single-Trial Analysis

To analyze single-trial data, we used GAMMs (Wood, 2017). We briefly introduce the main advantages and overall approach of the method. GAMMs are an extension of the generalized linear regression model in which nonlinear terms can be modeled jointly. They are more flexible than simple linear regression models as there is no requirement for a nonlinear function to be specified: The specific shape of the nonlinear function (i.e., smooth) is determined automatically. Specifically, the nonlinearities are modeled by so-called basis functions that consist of several low-level functions (linear, quadratic, etc.). We have chosen GAMMs as they can estimate the relationship between multiple predictors and the dependent variable using a nonlinear smooth function. The appropriate degrees of freedom and overfitting concerns are addressed through cross-validation procedures. Importantly, interactions between two nonlinear predictors can be modeled as well. In that case, the fitted function takes a form of a plane consisting of two predictors. Mathematically, this is accomplished by modeling tensor product smooths. Here, we used thin plate regression splines as they seemed most appropriate for large data sets and flexible fitting (Wood, 2003). In all presented analyses, we used a maximum likelihood method for smooth parameter optimization (Wood, 2011). GAMM analyses were performed using the *mgcv* R package (Version 1.8.12; Wood, 2009). GAMM results were plotted using the *itsadug* R package (Version 1.0.1; van Rij, Wieling, Baayen, & van Rijn, 2016).

Although not widely used, GAMMs are useful for modeling EEG data (Tremblay & Newman, 2015). Here, sensors were not included as fixed effects and the same model was fitted for every sensor separately. The resulting p values were corrected for multiple comparisons using false discovery rate correction (Genovese, Lazar, & Nichols, 2002). For plotting purposes, we averaged the data across significant sensors after false discovery rate correction and refitted the model. The specifics of this refitted model can be found in the tables. Besides typical F and p values, the tables contain the information on the estimated degrees of freedom (edf). edf Values can be interpreted as how much a given variable is smoothed. Although higher edf values indicate more complex splines, all tested models showed linear splines (edf = 1), depicted in the plotted model outcomes in associated figures.

We fitted the same GAMMs for several neurophysiological measurements chosen on the basis of previous literature. The fitted model contained a random effects term

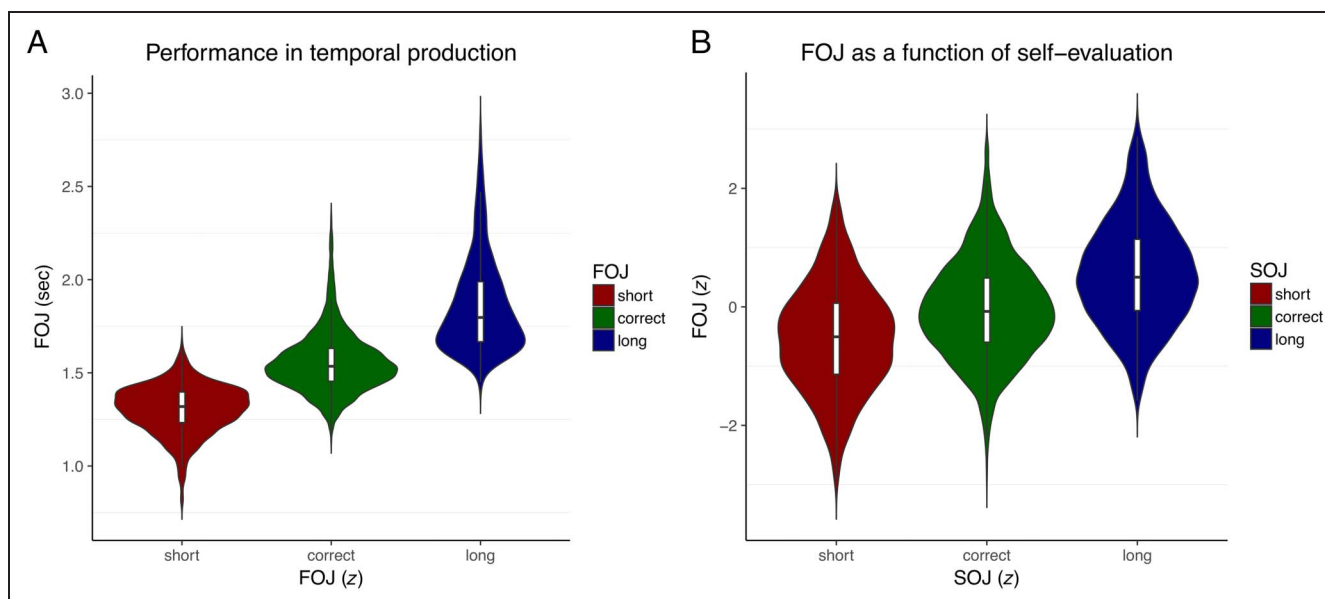


Figure 2. Temporal productions (FOJ) and self-evaluations (SOJ). (A) Participants accurately produced the target duration. The FOJ (first-order judgments) were clustered on the basis of the z-scored FOJ yielding the short, correct, and long categories. (B) The FOJ increased with increased SOJ indicating that participants could accurately self-evaluate (SOJ) their produced durations (FOJ).

for participant and fixed effects that were based on theoretical predictions. Specifically, the full model had the following specification: $\mu V/T/power \sim FOJ + SOJ + SOJ\ accuracy + FOJ \times SOJ + FOJ \times SOJ\ Accuracy$. Besides the random term for participants, the model contained smooth terms for the first- and second-order judgments, SOJ accuracy between the first- and second-order judgments, and the interaction term between FOJ and SOJ accuracy. Notably, FOJ, SOJ, and other predictors were entered as continuous variables in GAMM analyses as opposed to post hoc experimental conditions tested using cluster permutation, which suffered limitations from choosing arbitrary split point in the data.

The relative contribution of post-R2 components were tested similarly to the previous model. The full model had the following specification: $FOJ/SOJ \sim \alpha\ power + ERN + Pe$. Besides the random term for participants, the model contained smooth terms for all three included predictors. In the model outcomes, higher edf values (>1) indicate more complex splines. All tested models showed linear splines (edf = 1), depicted in the plotted model outcomes in associated figures.

Although GAMMs have built-in regularization procedures (meaning that they are somewhat inherently resistant against multicollinearity), multicollinearity can be assessed using variance inflation factor (VIF; *fmsb* R package, Version 0.5.2). Here, VIF was assessed for the final model and consisted in averaging data from multiple sensors collapsed over a particular variable at hand. None of the VIF values exceeded 1.1, indicating that multicollinearity was unlikely to have had a major influence on the reported findings. Note that Rogerson (2001) rec-

ommended a maximum VIF value of 5 and the author of *fmsb* recommended a value of 10.

Before entering empirical variables in the model, we calculated normalized values or z scores: Trials in which a given variable deviated more than 3 z scores were removed from further analysis. This normalization was computed separately for every MEG sensor and every EEG electrode. For single-trial analyses of β power in FOJ, we focused on the maximum power within the 0.4- to 0.8-sec period after the R1, similarly to the approach taken in Kononowicz et al. (2019). This time window overlapped with the selected time window that was used in cluster analyses. For the single-trial analyses of other brain signatures—that is, alpha power and sustained activity—we focused on the mean values in the time window of 0.4 sec after or preceding the R2.

RESULTS

Participants Track the Signed Magnitude of Just-Produced Time Intervals

Participants could accurately generate temporal productions (FOJ) with estimates centered around 1.5 sec. Figure 2A provides the normalized (z score) FOJ as a function of short, correct, and long categories defined according to each individual's temporal sensitivity (see Methods). To show that participants could accurately self-evaluate their FOJ, we sorted trials on the basis of their self-evaluations (SOJ). If FOJ and SOJ were independent, the FOJ sorted as a function of SOJ should not differ. Instead, we found the same linear trend when

we sorted FOJ as a function of SOJ (Figure 2B) as when we sorted FOJ as a function of FOJ (Figure 2A). This observation was statistically corroborated using a GAMM (Wood, 2017) with which we could assess whether SOJs were predictive of FOJs on a single-trial basis. The model fits confirmed that participants could correctly evaluate the signed error magnitude of their FOJ, $F(4.0) = 192.5$, $\text{edf} = 4.0$, $p < 10^{-15}$; that is, participants could correctly evaluate whether they were too short or too long and by how much. These results highlight the main behavioral effect subtending the question of TMC for subsequent analyses; complementary behavioral analyses can be found elsewhere (Kononowicz et al., 2019).

The Outline of Neuroimaging Data Analysis

We first performed a cluster analysis of the evoked and time–frequency activity, using FOJ and SOJ, which were binned as factors. We then performed single-trial analyses, in which FOJs and SOJs were used as continuous predictors. This series of tests was followed by single-trial analyses using models predictive of FOJs or SOJs to assess the relative contributions of evoked and oscillatory power activity within the same statistical model. Using a single-trial approach, we could thus assess the link between β power (internal variable coding for duration [Kononowicz et al., 2019; Wiener, Parikh, Krakow, & Coslett, 2018; Kulashkhar, Pekkola, Palva, & Palva, 2016; Kononowicz & Van Rijn, 2015]) and the postinterval production signatures (i.e., the post-R2 activity). Last, we assessed whether participants had access to temporal information before the termination of their temporal production, by analyzing brain activity locked to R2 during the temporal production.

ERN/Pe is Not Sensitive to the Temporal Dimension of Motor Action

The ERN and the Pe are seminal electrophysiological signatures of error monitoring and self-evaluation. The ERN is characterized by a large negative, and the Pe, a positive, evoked response occurring 0.1–0.3 sec after an error (Yeung, Botvinick, & Cohen, 2004; Holroyd & Coles, 2002). The ERN/Pe complex is obtained by subtracting error trials from correct trials. In our time production task, incorrect trials could either be too short and too long. The hypothesis that ERN/Pe could reflect a response selection error in the temporal domain (e.g., Luu et al., 2000) thus predicted a V-shaped amplitude pattern so that the further away the temporal production was from the target duration, the larger the amplitude of the ERN/Pe would be. In other words, the larger the error, the larger the ERN/Pe amplitude irrespective of the sign of the error.

To test this hypothesis, we looked at the evoked responses after the termination of the temporal production, that is, the R2-locked evoked activity. First, we observed a negative component peaking ~60 msec post-R2, which seemed characteristic of an early postmovement

activity (Praamstra et al., 2003) in both EEG and MEG (Figure 3A and C and Figure 3B and D, respectively). This component was followed by a positive evoked potential (Pe). To test the possible sensitivity of the presumed ERN/Pe to temporal error, we used spatiotemporal cluster permutation tests of EEG and MEG evoked responses. We first compared the evoked responses after the production of the time interval (0–0.4 sec post-R2) as a function of

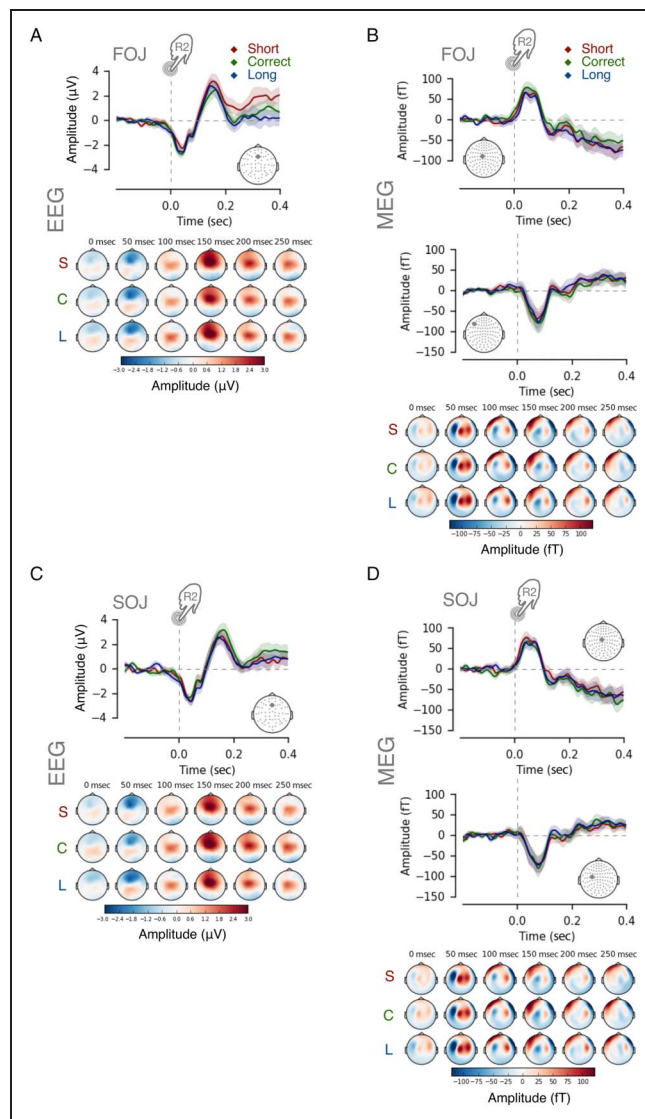
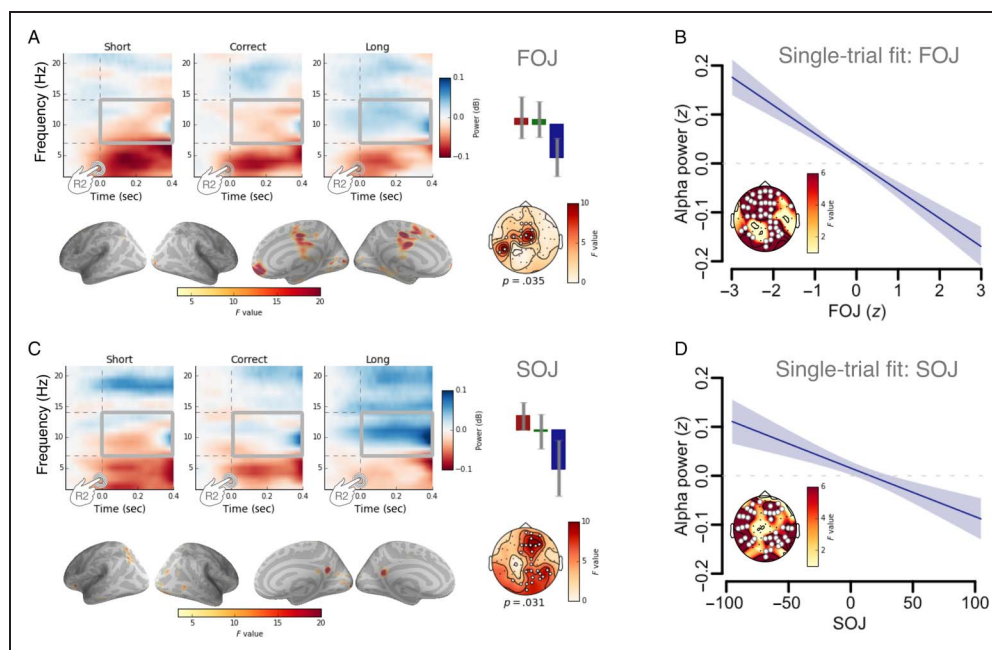


Figure 3. No evidence for ERN-like responses. ERPs/ERFs up to 0.4 sec after the termination of the produced duration (R2). The top displays the evoked responses as a function of FOJ (A, B), whereas the bottom displays the data as a function of SOJ (C, D), as indicated by the gray insets in the top left part of every panel. The evoked responses showed no significant differences in amplitude or latency as a function of FOJ or SOJ. Time courses illustrate the evoked responses from the gray EEG electrode or MEG sensor in the topographical map inset. Colored topographical maps display the evoked responses for short (S: red), correct (C: green), and long (L: blue) categories. The EEG time course at Fz was reported as a function of (A) FOJ and (C) SOJ categories, respectively. Two MEG sensors are reported as a function of (B) FOJ and (D) SOJ categories.

Figure 4. Post-R2 α power signatures of FOJ and SOJ.

(A) Time–frequency spectra for one EEG electrode (Cz), with the highest F value, illustrating the outcomes of a cluster-based permutation F test capturing a decrease of α power (8–14 Hz) as a function of FOJ categories. The average α power in the highlighted time–frequency window (gray squares) significantly decreased with increasing duration production (bar plot: red indicates short, green indicates correct, and blue indicates long). (B) The single-trial model fit. Post-R2 α power decreased as a function of FOJ. Statistical details in Table 1. (C) Time–frequency spectra for the Fz EEG electrode with the largest F value (cluster-based permutation test). Bar plot illustrating the average α power as a function of SOJ categories: α power decreased with increasing SOJ. Source estimates of the α power effect as a function of SOJ (uncorrected F map; combined M/EEG) implicated medio-central and prefrontal cortices. The strongest source originated from the precuneus. (D) The single-trial model fit. Post-R2 α power decreased as a function of SOJ. Statistical details in Table 2.



FOJ and SOJ. In Figure 3, the top panels display the data as a function of FOJ (Figure 3A and B); and the bottom panels, as a function of SOJ (Figure 3C and D). The spatiotemporal cluster permutation tests yielded no significant changes in evoked responses as a function of FOJ (Figure 3A and B) or SOJ (Figure 3C and D), whether in EEG (Figure 3A and C; all p s > .1) or in MEG (Figure 3B and D; all p s > .1).

We next compared the time–frequency activity after short, correct, and long trials (post-R2: 0–0.4 sec). In the remaining analyses, we solely focused on EEG activity, which is more sensitive to activity in midline structures such as cingulate cortices. Recent work on cognitive control has suggested a link between ERN and theta oscillations (θ : 3–7 Hz) sharing common mid-frontal neural generators (Cavanagh & Frank, 2014;

Table 1. The Results of Single-Trial GAMM Analysis Based on α Power after the Second Keypress

| <i>Parametric Coefficients</i> | <i>Estimate</i> | <i>Std. Error</i> | <i>t Value</i> | <i>p Value</i> |
|--------------------------------|-----------------|-------------------|----------------|-------------------|
| Intercept | 0.0042 | 0.0086 | 0.4870 | .6262 |
| <i>Smooth Terms</i> | | | | |
| s(FOJ) | 1.0000 | 1.0001 | 22.9395 | <.0001* |
| s(SOJ) | 1.0000 | 1.0001 | 0.3052 | .5807 |
| s(SOJ accuracy) | 1.0001 | 1.0002 | 0.0775 | .7809 |
| ti(FOJ \times SOJ) | 1.0012 | 1.0025 | 0.0019 | .9650 |
| ti(FOJ \times SOJ Accuracy) | 1.0009 | 1.0018 | 3.9561 | .0466 |
| s(participant) | 0.0012 | 11.0000 | 0.0000 | .9999 |

GAMM analysis: R2-locked α power, FOJ cluster, full model

The table displays the results of the model that was based on the data collapsed across the significant sensors, showing the main effect of FOJ, when the model was fitted on a per-sensor basis. Although FOJ \times SOJ Accuracy reached significance level in the refitted model, it was not significant in the first step where model was assessed for each individual sensor and p values were corrected (see Single-trial analysis).

The asterisk signifies the factors that were significant after false discovery rate correction, applied after the same model was fitted for every sensor separately.

Table 2. The Results of Single-Trial GAMM Analysis Based on α Power after the Second Keypress

| Parametric Coefficients | Estimate | Std. Error | <i>t</i> Value | <i>p</i> Value |
|-------------------------------|---------------|---------------|----------------|----------------|
| Intercept | 0.0045 | 0.0080 | 0.5651 | .5720 |
| <i>Smooth Terms</i> | | | | |
| s(SOJ) | 1.0001 | 1.0003 | 12.3827 | .0004* |
| s(SOJ accuracy) | 1.0032 | 1.0064 | 0.4280 | .5179 |
| ti(FOJ \times SOJ) | 1.0016 | 1.0033 | 0.2936 | .5888 |
| ti(FOJ \times SOJ Accuracy) | 2.1676 | 2.6620 | 2.2540 | .1042 |
| s(participant) | 0.0012 | 11.0000 | 0.0000 | .9994 |

GAMM analysis: R2-locked α power, SOJ cluster, model without FOJ term

The table displays the results of the model that was based on the data collapsed across the significant sensors, showing the main effect of SOJ, when the model was fitted on a per-sensor basis and the FOJ term has been excluded from the model.

The asterisk signifies the factors that were significant after false discovery rate correction, applied after the same model was fitted for every sensor separately.

Cohen & Cavanagh, 2011). We thus explored evoked θ activity from 0 to 0.2 sec post-R2. We constrained the analysis window from 0.2 to 0.4 sec post-R2 to prevent capturing spurious evoked activity, which could mask brain activity specific to the self-evaluation of temporal error. As for the ERN/Pe, our prediction was that stronger θ power would indicate larger temporal errors irrespective of their sign. A cluster permutation test of the θ band power yielded no significant effect of FOJ or SOJ ($p > .1$). A post hoc spatiotemporal cluster permutation test showed no significant effects in β (14–40 Hz) or γ (>40 Hz) frequency ranges as a function of FOJ ($p > .1$) or SOJ ($p > .1$). Hence, we found no evidence for a V-shaped pattern of the evoked responses as a function of FOJ or SOJ in the ERN or in a frequency band that could support the TED hypothesis in this experimental paradigm.

Postinterval Oscillatory Activity as Readout

While assessing oscillatory activity after the termination of the time interval, we observed a significant cluster in the alpha-band power (α : 8–14 Hz) as a function of FOJ categories (Figure 4A, $p = .035$). The main sources of this effect originated in medial and prefrontal cortices (Figure 4A, bottom row). Similarly, a significant effect of α power was found as a function of SOJ categories (Figure 4C, $p = .031$). On a given trial, the shorter the self-evaluation, the larger the α power (Figure 4C).

We tested the possibility of a linear relation between the observed α power and the behavioral variables using a single-trial analysis of the normalized mean α power. The single-trial model used the set of behavioral variables to predict α power (0–0.4 sec post-R2): Among other predictors, we used SOJ and FOJ (see Single-trial analysis). The analysis revealed a consistent pattern across two

factors, one associated with FOJ and the other with SOJ: The first significant group of electrodes showed a linear relationship between α power and FOJ ($F = 22.9$, $edf = 1$, $p < .0001$; Figure 4B, Table 1) so that shorter trials were associated with a larger α power (i.e., the shorter the temporal production, the stronger the α power). Consistent with the topographical scalp differences, the neural contributors of α power changes in FOJ were distinct from those observed in SOJ (Figure 4A

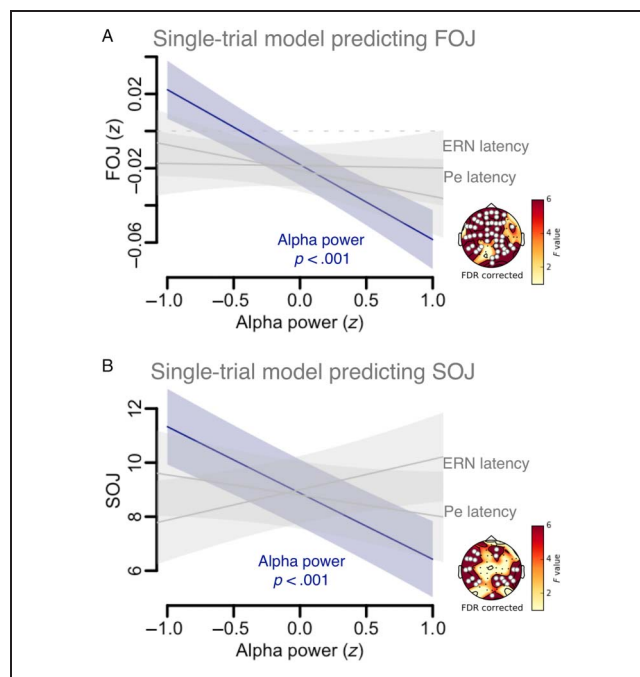


Figure 5. α Power contributes to SOJ and to FOJ. Single-trial statistical model fit predicting FOJ (A) and SOJ (B) using α power, and evoked activity amplitude at predicted ERN and Pe latencies. The topographical map shows the distribution of significant EEG electrodes.

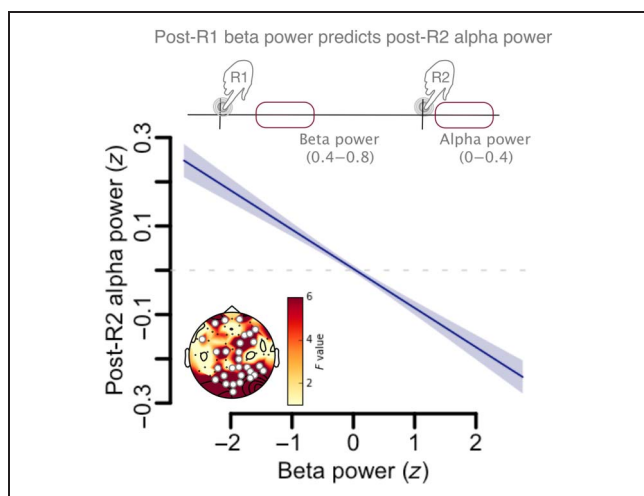


Figure 6. Post-R1 power contributes to post-R2 evaluation. Single-trial model fit predicting post-R2 α power using the post-R1 power. The topographical map shows the distribution of significant EEG electrodes.

and C, bottom): Source estimates for the FOJ effect were found in medial, central, and prefrontal cortices, whereas those for the SOJ effect were located near the precuneus cortices.

Considering the anatomical separability of the neural generators, we refitted the single-trial model without the FOJ term, which accounted for most of the variance when the full model was considered (Figure 4B, Table 1). As SOJ and FOJ were correlated, we expected that removing the FOJ term would allow to show the SOJ impact and we hypothesized that this refitted model would show a different topography than the model including the FOJ term. This analysis revealed a significant group of electrodes for which α power was linearly predictive of SOJ ($F = 12.4$, $edf = 1$, $p = .0004$; Figure 4D, Table 2).

Both the analysis using categorical responses (i.e., data binning as short/correct/long) and the single-trial model thus indicated that the FOJ and SOJ effects were topographically distinct, in agreement with the source estimations (Figure 4C, bottom).

Table 3. GAMM Analysis: Beta Power Predicting Post-R2 Alpha

| Parametric Coefficients | Estimate | Std. Error | <i>t</i> Value | <i>p</i> Value |
|------------------------------------|---------------|---------------|----------------|-------------------|
| (Intercept) | 0.0034 | 0.0079 | 0.4275 | .6691 |
| Smooth Terms | <i>edf</i> | <i>Ref.df</i> | <i>F Value</i> | <i>p Value</i> |
| s(β power) | 1.0002 | 1.0004 | 44.5739 | <.0001* |
| s(participant) | 0.0032 | 11.0000 | 0.0000 | 1.0000 |

GAMM analysis: β predicting post-R2 alpha

The results of single trial GAMM analysis where β power was tested as a predictor for post-R2 α . The table displays the results for the final model that was based on the data collapsed across the significant sensors.

The asterisk signifies the factors that were significant after false discovery rate correction, applied after the same model was fitted for every sensor separately.

After the end of the temporal production (post-R2), changes in α power seemed indicative of the signed magnitude difference between the target interval and the produced time interval. We speculated that a readout activity would linearly code for the state of the networks related to duration estimation at the outset of the produced interval. Indeed, the linear trend of α power, together with distinct generators of FOJ and SOJ effects, appeared in line with the TMC readout hypothesis. Considering that an important goal for this work was to compare the predictions of TED against those of TMC (and not the evaluation of TED or TMC per se), we next ran a single-trial analysis that directly tested the contributions of TED and TMC.

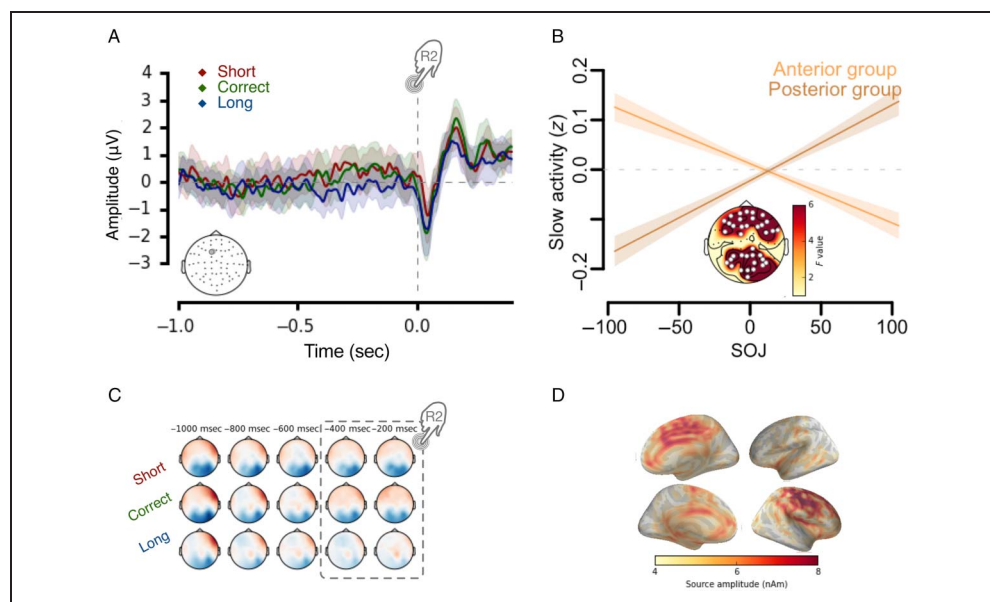
Relative Contributions of Evoked Activity and α Power to Temporal Error Monitoring

Considering the hypothetical ERN/Pe predicted by TED and the α power observed in exploratory analysis, we assessed the relative contribution of evoked and oscillatory activity to the self-evaluation of a generated duration. Using a single-trial analysis, we assessed a model in which FOJ or SOJ was predicted by three factors: evoked activity at the predicted ERN/Pe latencies and α power. The associated temporal windows were 0–0.1, 0.1–0.3, and 0–0.4 sec, respectively. These latencies typically predict the ERN and Pe in the literature, whereas no a priori window could be defined for oscillatory power. The analysis revealed that the only contributing factor to FOJ ($F = 12.8$, $edf = 1$, $p = .0003$; Figure 5A) and SOJ ($F = 14.1$, $edf = 1$, $p = .0004$; Figure 5B) was α power. We thus explored further the notion that a linear scaling with SOJ may index a readout mechanism during TMC.

β Power Timing Signature Is Consistent with Post-R2 α Scaling

As previous studies have suggested that β power was strongly associated with an internal variable coding for

Figure 7. Sustained activity before R2 indicative of SOJ. (A) Time courses and topographical plots of EEG activity 1 sec before the second keypress as a function of SOJ. The electrode location is displayed in the bottom left corner. (B) Single-trial model fit. The sustained brain activity preceding the R2 (−0.4 to 0 sec) predicted SOJ. The anterior and posterior clusters were plotted separately because of reversed polarities of EEG signals depicted in C. Statistical details in Tables 3 and 4. (C) Topographical maps show scalp voltage distribution 1 sec before the R2. (D) Cortical source estimates collapsed over all conditions. Motor and midfrontal regions were the most likely origins of the sustained activity.



duration during time estimation (Kononowicz et al., 2019; Wiener et al., 2018), the post-R2 activity may be linked to β power during timing. To directly test this hypothesis, we assessed whether β power after the first keypress (R1) predicted the postinterval α power. This analysis showed that β power during temporal production (post-R1) was significantly predictive of α power after temporal production (post-R2) in frontal and posterior sensors ($F = 44.6$, $edf = 1$, $p < .0001$; Figure 6, Table 3). This effect suggested that β power at the onset of the temporal production could be used for the post-interval α modulation (readout). Hence, this observation supports an interpretation in which the linear

scaling between post-R2 α power and SOJ, as a marker of self-estimation, relies on an internal variable coding for duration (β power) during the FOJ.

No Evidence of Self-evaluation before R2

The accurate estimation of signed temporal errors suggested that participants could access their temporal errors. We thus asked whether such self-evaluation already started before the completion of the time interval, that is, before R2. Similar to the previous post-R2 analyses, we contrasted evoked activity and α power as a function of FOJ and SOJ, but this time, from −0.4 to

Table 4. The Results of Single-Trial GAMM Analysis Based on Sustained Activity Preceding the Second Keypress

| <i>Parametric Coefficients</i> | <i>Estimate</i> | <i>Std. Error</i> | <i>t Value</i> | <i>p Value</i> |
|--------------------------------|-----------------|-------------------|----------------|-------------------|
| <i>Intercept</i> | −0.0009 | 0.0072 | −0.1318 | .8951 |
| <i>Smooth Terms</i> | <i>edf</i> | <i>Ref.df</i> | <i>F Value</i> | <i>p Value</i> |
| s(FOJ) | 1.0001 | 1.0001 | 0.3260 | .5680 |
| s(SOJ) | 1.0002 | 1.0003 | 20.5239 | <.0001* |
| s(SOJ accuracy) | 1.0002 | 1.0005 | 1.0091 | .3151 |
| ti(SOJ × FOJ) | 1.0027 | 1.0055 | 0.8087 | .3700 |
| ti(FOJ × SOJ Accuracy) | 1.0089 | 1.0178 | 1.3847 | .2368 |
| s(participant) | 0.0015 | 11.0000 | 0.0000 | .9948 |

GAMM analysis: R2-locked readiness potential, anterior cluster

The table displays the results for the final model that was based on the data collapsed across the significant sensors, showing the main effect of SOJ, when the model was fitted on a per-sensor basis. The table depicts the anterior cluster.

The asterisk signifies the factors that were significant after false discovery rate correction, applied after the same model was fitted for every sensor separately.

Table 5. The Results of Single-Trial GAMM Analysis Based on Sustained Activity Preceding the Second Keypress

| <i>Parametric Coefficients</i> | <i>Estimate</i> | <i>Std. Error</i> | <i>t Value</i> | <i>p Value</i> |
|--------------------------------|-----------------|-------------------|----------------|-------------------|
| (Intercept) | −0.0040 | 0.0074 | −0.5389 | .5900 |
| <i>Smooth Terms</i> | | | | |
| | <i>edf</i> | <i>Ref.df</i> | <i>F value</i> | <i>p Value</i> |
| s(FOJ) | 1.0000 | 1.0001 | 0.1091 | .7412 |
| s(SOJ) | 1.0000 | 1.0001 | 27.6527 | <.0001* |
| s(SOJ accuracy) | 1.0000 | 1.0001 | 4.4611 | .0347 |
| ti(SOJ × FOJ) | 2.0365 | 2.5519 | 1.3882 | .2115 |
| ti(FOJ × SOJ Accuracy) | 1.0077 | 1.0153 | 1.0731 | .2974 |
| s(participant) | 0.0003 | 11.0000 | 0.0000 | .9815 |

GAMM analysis: R2-locked readiness potential, posterior cluster

The table displays the results for the final model that was based on the data collapsed across the significant sensors, showing the main effect of SOJ, when the model was fitted on a per-sensor basis. The table depicts the posterior cluster.

The asterisk signifies the factors that were significant after false discovery rate correction, applied after the same model was fitted for every sensor separately.

0 sec post-R2 (Figure 7A). First, no significant variation of α band power was found. Second, a trial-by-trial analysis revealed a significant effect of SOJ on the amplitude of evoked activity (Figure 7B): Anterior and posterior clusters with positive and negative voltages (Figure 7B) covaried with SOJ such that the positive frontal cluster ($F = 20.5$, $edf = 1$, $p < .0001$; Figure 7B, Table 4) negatively covaried with SOJ (Figure 7B and C) and the posterior negative cluster positively covaried with SOJ ($F = 27.7$, $edf = 1$, $p < .0001$; Figure 7B, Table 5). In line with this bipolar EEG scalp distribution, and in agreement with previous work (Figure 7C; Wiener, Turkeltaub, & Coslett, 2010), brain sources at the origin of this activity were located in the motor, premotor, and midfrontal cortices (Figure 7D).

As only SOJ covaried with slow evoked activity, we hypothesized that the sustained activity may reflect an intrinsic decisional bias affecting self-evaluation, which would be functionally distinct from the representation of duration that would involve both FOJ and SOJ. This effect of SOJ is also in line with the notion that participants have no access to temporal errors before R2: Although we previously reported that β power during temporal production predicted FOJ, whether an agent can act upon that representation before R2 should be further investigated.

In summary, we identified cortical signatures of self-evaluation in temporal production. Postinterval α power was linked to preceding β power, suggesting the evaluation of an internal variable coding for duration as previously suggested by the accurate representation of individuals' temporal uncertainties (Balci et al., 2009).

DISCUSSION

We assessed two working hypotheses on the neuronal correlates and mechanisms supporting the evaluation of

self-generated time intervals (TED and TMC), using a task in which participants produced durations, and evaluated the signed error magnitude of their time estimates while being recorded with combined M/EEG. We found no robust evidence for the generation of an ERN/Pe modulated as a function of temporal error in this task. However, we found that α power after R2 negatively correlated with SOJs and with FOJs. We interpret these findings as evidence in favor of the TMC working hypothesis. In support of the TMC hypothesis, the initial β power, known to scale with the duration of a produced time interval in this task (Kononowicz et al., 2019), predicted the changes in α power after the produced time interval. Below, we discuss these interpretations together with the current shortcomings of our study.

Temporal Metarepresentations

TMC posits the existence of a process that actively infers the state of duration representation, that is, the meta-representation of a duration (van Wassenhove, 2009; Cleeremans, Timmermans, & Pasquali, 2007). What crucially follows is that the metarepresentation of duration would be specified by neural signatures that would be anatomically and functionally distinct from the neural signatures of the duration representation (Lak et al., 2014). In line with this, the cortical generators for the post-R2 α power and the post-R1 β power were clearly distinguishable (Kononowicz et al., 2019), fulfilling the criterion of anatomical separability between the first- and second-order representations of duration. In addition, both α and β neural oscillatory activity have typically been ascribed different functional roles: α tends to be implicated in the regulation of a global network (Palva & Palva, 2012), whereas β is implicated in the representation of

sensorimotor features (Kilavik, Zaepffel, Brovelli, MacKay, & Riehle, 2013; Engel & Fries, 2010). Complementary to these two functional roles, a strong α - β coupling was shown to monitor the timing precision in this task (Grabot et al., 2019).

Indirect evidence has suggested the existence of metacognitive mechanisms that required either a passive or an active readout (Fleming & Daw, 2017): A passive sensitivity to the state of the system automatically detects temporal delays in motor action (in line with the TED hypothesis), or an active process implies a process of inferring of the state of duration representation (in line with the TMC hypothesis). Here, we suggest that the decrease in α power after the production of a duration may reflect the outcome of an active readout process. This working hypothesis is also quite testable: If the metacognitive readout is an active process, the absence of self-evaluation in a task should abolish the post-R2 α as a function of duration category. One limitation of this study was that there were no trials in which participants did not self-evaluate their time production. Fortunately, previous EEG work assessing time reproduction tasks in the absence of metacognitive inference (Kononowicz & Van Rijn, 2015; Figures 4 and 5, bottom) showed no post-R2 α or theta power changes as a function of duration category. Thus, changes in post-R2 α may only be seen when participants are explicitly asked to self-evaluate their temporal performance. Future experiments should assess under which conditions self-evaluation is a function of an active inference or a plausible passive dependency between duration representation and error monitoring variable.

Additional evidence supports the idea that first-order signals could be read out by second-order areas of brain regions. For example, the pulvinar neurons have been shown to encode confidence (second-order variable) independently of other areas processing first-order variables (Komura, Nikkuni, Hirashima, Uetake, & Miyamoto, 2013): This study suggested that one population of neurons can read out the activity of neural population encoding primary sensory variables. Other studies have also suggested that particular brain regions independently code for first- and second-order signals (Lak et al., 2014). In humans, similar notions have been explored: Using TMS, prefrontal areas have been shown to read out the strength of perceptual signals in service of confidence judgments (Shekhar & Rahnev, 2018). In line with these ideas, the mapping between β power and duration may be realized via networking through higher-order brain regions. For example, pFC, implicated in timing (Kim et al., 2017), could monitor signals in motor cortex (Narayanan & Laubach, 2006) or the cortico-basal ganglia loop. Indeed, the cortical sources observed in our study were consistent with the acknowledged role of midline cingulate regions in self-monitoring (Miyamoto et al., 2017) and error monitoring (Ullsperger, Fischer, Nigbur, & Endrass, 2014). Moreover, the orbito-frontal and posterior cingulate were implicated in the metacognitive performance: The association between FOJ and α power originated from pFCs and ACC, whereas the

association between SOJ and α power implicated the precuneus, which has been reported during confidence judgments (Ye, Zou, Lau, Hu, & Kwok, 2018; De Martino, Fleming, Garrett, & Dolan, 2013) and error processing (Menon, Adelman, White, Glover, & Reiss, 2001). Gray matter volume in precuneus predicts introspective accuracy (Fleming, Weil, Nagy, Dolan, & Rees, 2010) and metacognitive efficiency in memory (McCurdy et al., 2013).

What Signals Could Be Read Out

Previous studies reported that β power scaled with the length of produced interval (Kononowicz et al., 2019; Kononowicz & Van Rijn, 2015) and that the degree of separation in β power state trajectories predicted individuals' temporal metacognitive performance (Kononowicz et al., 2019). If β power conveys information about the representation of duration, we hypothesized that it could also serve as a signature for the readout: Congruent with this, β power predicted the post-R2 α power in our study. The effects in α power suggest that the monitoring of internal states could rely on different sources of information than only β power, and two studies further support this notion. First, α oscillations have been implicated in performance monitoring when task errors relied more on the attentional lapses than on the lack of executive control over the motor system (van Driel, Ridderinkhof, & Cohen, 2012). Second, participants can monitor their attentional state, which is indexed by the lateralization pattern of α oscillations (Whitmarsh, Barendregt, Schoffelen, & Jensen, 2014). The post-R2 α decrease observed here could also be interpreted as a reorienting of attention after the generation of durations that were too long. Specifically, in an attentional gate model of time perception (Zakay & Block, 1995), long durations would correspond to not enough attention paid to temporal production, hence more attention needed for the next trial. However, the lack of association between α power during the self-generation of durations and produced duration in this data set (Kononowicz et al., 2019) and in previous studies (Kononowicz & Van Rijn, 2015) does not fit well with this interpretation. Whether α power could contribute to metacognitive performance in the timing of longer durations thus remains to be tested. Future studies should extend the range of tested durations to longer as well as shorter ones. A better assessment on an extended range of durations would allow evaluating the relevance of the current findings to different timing mechanisms (Lewis & Miall, 2003).

Another open question is why readout-related processes and self-monitoring would implicate α oscillations. When assessing the role of cross-frequency coupling in this timing task, we found that the coupling strength between the phase of α oscillations and the power of β oscillations was indicative of the precision with which participants produced a duration (Grabot et al., 2019). This pattern was found during the generation of the

interval. One speculative hypothesis is that the termination of the interval (R2) may implicate the readout of the precision maintained in the coupling of β power with respect to the phase of alpha. This mechanism would be close to the prediction of oscillatory-based mechanisms in event timing, which implicate the phase of oscillations in timing precision (Gallistel, 1990). This, however, remains an open and very difficult question to address empirically, one for which a set of dedicated experiments—including animal work—would be needed.

Why Do Participants Not Correct Temporal Errors in the Presence of Temporal Information?

Although previous reports suggest that temporal information coded by β power is present at the interval onset, it is not clear when that information is accessible for the inference of temporal errors: already before or only after R2? Only SOJ predicted changes in slow evoked activity before R2. As FOJ did not predict slow evoked activity, this information did not appear relevant to the termination of R2, suggesting that slow activity biases SOJ, without FOJ contribution. Together with the post-R2 α power scaling with FOJ and SOJ, our results suggest that participants may only have access to their temporal errors post-R2. Notably, the notion of readout is not equivalent with the access to temporal information before R2. However, it is a viable possibility that the readout process is initialized before the R2, the results of which become accessible after the R2.

Acknowledgments

This work was supported by an ERC-YStG-263584, an ANR10JCJC-1904, and an ANR-16-CE37-0004-04 to V. v. W. We thank the members of UNIACT and the medical staff at NeuroSpin for their help in recruiting and scheduling participants. We thank Clémence Roger for her initial contributions to the study and members of UNICOG for fruitful discussions. Preliminary results were presented at Society for Neuroscience (2016).

Reprint requests should be sent to Tadeusz W. Kononowicz, CEA/DRF NeuroSpin - INSERM Cognitive Neuroimaging Unit, Bât 145 Point Courrier 156, Gif s/Yvette F-91191, France, or via e-mail: t.w.kononowicz@icloud.com.

REFERENCES

- Akdoğan, B., & Balci, F. (2017). Are you early or late?: Temporal error monitoring. *Journal of Experimental Psychology: General*, *146*, 347–361.
- Balci, F., Freestone, D., & Gallistel, C. R. (2009). Risk assessment in man and mouse. *Proceedings of the National Academy of Sciences, U.S.A.*, *106*, 2459–2463.
- Bell, A. J., & Sejnowski, T. J. (1995). An information-maximization approach to blind separation and blind deconvolution. *Neural Computation*, *7*, 1129–1159.
- Brainard, D. H. (1997). The psychophysics toolbox. *Spatial Vision*, *10*, 433–436.
- Cavanagh, J. F., & Frank, M. J. (2014). Frontal theta as a mechanism for cognitive control. *Trends in Cognitive Sciences*, *18*, 414–421.
- Cleeremans, A., Timmermans, B., & Pasquali, A. (2007). Consciousness and metarepresentation: A computational sketch. *Neural Networks*, *20*, 1032–1039.
- Cohen, M. X. (2014). A neural microcircuit for cognitive conflict detection and signaling. *Trends in Neurosciences*, *37*, 480–490.
- Cohen, M. X., & Cavanagh, J. F. (2011). Single-trial regression elucidates the role of prefrontal theta oscillations in response conflict. *Frontiers in Psychology*, *2*, 30.
- Dale, A. M., Liu, A. K., Fischl, B. R., Buckner, R. L., Belliveau, J. W., Lewine, J. D., et al. (2000). Dynamic statistical parametric mapping: Combining fMRI and MEG for high-resolution imaging of cortical activity. *Neuron*, *26*, 55–67.
- De Martino, B., Fleming, S. M., Garrett, N., & Dolan, R. J. (2013). Confidence in value-based choice. *Nature Neuroscience*, *16*, 105–110.
- Engel, A. K., & Fries, P. (2010). Beta-band oscillations—Signaling the status quo? *Current Opinion in Neurobiology*, *20*, 156–165.
- Falkenstein, M., Hohnsbein, J., Hoormann, J., & Blanke, L. (1991). Effects of crossmodal divided attention on late ERP components. II. Error processing in choice reaction tasks. *Electroencephalography and Clinical Neurophysiology*, *78*, 447–455.
- Foote, A. L., & Crystal, J. D. (2007). Metacognition in the rat. *Current Biology*, *17*, 551–555.
- Flavell, J. H. (1979). Metacognition and cognitive monitoring: A new area of cognitive–developmental inquiry. *American Psychologist*, *34*, 906–911.
- Fleming, S. M., & Daw, N. D. (2017). Self-evaluation of decision-making: A general Bayesian framework for metacognitive computation. *Psychological Review*, *124*, 91–114.
- Fleming, S. M., & Dolan, R. J. (2012). The neural basis of metacognitive ability. *Philosophical Transactions of the Royal Society of London, Series B, Biological Sciences*, *367*, 1338–1349.
- Fleming, S. M., Dolan, R. J., & Frith, C. D. (2012). Metacognition: Computation, biology and function. *Philosophical Transactions of the Royal Society of London, Series B, Biological Sciences*, *367*, 1280–1286.
- Fleming, S. M., Weil, R. S., Nagy, Z., Dolan, R. J., & Rees, G. (2010). Relating introspective accuracy to individual differences in brain structure. *Science*, *329*, 1541–1543.
- Fischl, B., Salat, D. H., van der Kouwe, A. J., Makris, N., Ségonne, F., Quinn, B. T., et al. (2004). Sequence-independent segmentation of magnetic resonance images. *Neuroimage*, *23*, S69–S84.
- Gallistel, C. R. (1990). *The organization of learning*. Cambridge, MA: MIT Press.
- Gehring, W. J., Goss, B., Coles, M. G. H., Meyer, D. E., & Donchin, E. (1993). A neural system for error detection and compensation. *Psychological Science*, *4*, 385–390.
- Genovese, C. R., Lazar, N. A., & Nichols, T. (2002). Thresholding of statistical maps in functional neuroimaging using the false discovery rate. *Neuroimage*, *15*, 870–878.
- Grabot, L., Kononowicz, T. W., La Tour, T. D., Gramfort, A., Doyère, V., & van Wassenhove, V. (2019). The strength of alpha-beta oscillatory coupling predicts motor timing precision. *Journal of Neuroscience*, *39*, 3277–3291.
- Gramfort, A., Luessi, M., Larson, E., Engemann, D. A., Strohmeier, D., Brodbeck, C., et al. (2014). MNE software for processing MEG and EEG data. *Neuroimage*, *86*, 446–460.
- Holroyd, C. B., & Coles, M. G. (2002). The neural basis of human error processing: Reinforcement learning, dopamine, and the error-related negativity. *Psychological Review*, *109*, 679–709.
- Ivry, R. B., & Schlerf, J. E. (2008). Dedicated and intrinsic models of time perception. *Trends in Cognitive Sciences*, *12*, 273–280.

- Jantzen, K. J., Ratcliff, B. R., & Jantzen, M. G. (2018). Cortical networks for correcting errors in sensorimotor synchronization depend on the direction of asynchrony. *Journal of Motor Behavior, 50*, 235–248.
- Jovicich, J., Czanner, S., Greve, D., Haley, E., van der Kouwe, A., Gollub, R., et al. (2006). Reliability in multi-site structural MRI studies: Effects of gradient non-linearity correction on phantom and human data. *Neuroimage, 30*, 436–443.
- Karmarkar, U. R., & Buonomano, D. V. (2007). Timing in the absence of clocks: Encoding time in neural network states. *Neuron, 53*, 427–438.
- Kilavik, B. E., Zaepffel, M., Brovelli, A., MacKay, W. A., & Riehle, A. (2013). The ups and downs of β oscillations in sensorimotor cortex. *Experimental Neurology, 245*, 15–26.
- Kim, Y. C., Han, S. W., Alberico, S. L., Ruggiero, R. N., De Corte, B., Chen, K. H., et al. (2017). Optogenetic stimulation of frontal D1 neurons compensates for impaired temporal control of action in dopamine-depleted mice. *Current Biology, 27*, 39–47.
- Komura, Y., Nikkuni, A., Hirashima, N., Uetake, T., & Miyamoto, A. (2013). Responses of pulvinar neurons reflect a subject's confidence in visual categorization. *Nature Neuroscience, 16*, 749–755.
- Kononowicz, T. W., Roger, C., & van Wassenhove, V. (2019). Temporal metacognition as the decoding of self-generated brain dynamics. *Cerebral Cortex, 29*, 4366–4380.
- Kononowicz, T. W., & van Rijn, H. (2015). Single trial β oscillations index time estimation. *Neuropsychologia, 75*, 381–389.
- Kulashekhar, S., Pekkola, J., Palva, J. M., & Palva, S. (2016). The role of cortical beta oscillations in time estimation. *Human Brain Mapping, 37*, 3262–3281.
- Laje, R., & Buonomano, D. V. (2013). Robust timing and motor patterns by taming chaos in recurrent neural networks. *Nature Neuroscience, 16*, 925–933.
- Lak, A., Costa, G. M., Romberg, E., Koulakov, A. A., Mainen, Z. F., & Kepecs, A. (2014). Orbitofrontal cortex is required for optimal waiting based on decision confidence. *Neuron, 84*, 190–201.
- Levitt, H. (1971). Transformed up-down methods in psychoacoustics. *Journal of the Acoustical Society of America, 49*, 467–477.
- Lewis, P. A., & Miall, R. C. (2003). Distinct systems for automatic and cognitively controlled time measurement: Evidence from neuroimaging. *Current Opinion in Neurobiology, 13*, 250–255.
- Luu, P., Flaisch, T., & Tucker, D. M. (2000). Medial frontal cortex in action monitoring. *Journal of Neuroscience, 20*, 464–469.
- Maris, E., & Oostenveld, R. (2007). Nonparametric statistical testing of EEG- and MEG-data. *Journal of Neuroscience Methods, 164*, 177–190.
- Marti, S., Sackur, J., Sigman, M., & Dehaene, S. (2010). Mapping introspection's blind spot: Reconstruction of dual-task phenomenology using quantified introspection. *Cognition, 115*, 303–313.
- McCurdy, L. Y., Maniscalco, B., Metcalfe, J., Liu, K. Y., de Lange, F. P., & Lau, H. (2013). Anatomical coupling between distinct metacognitive systems for memory and visual perception. *Journal of Neuroscience, 33*, 1897–1906.
- Meckler, C., Allain, S., Carbonnell, L., Hasbroucq, T., Burle, B., & Vidal, F. (2010). Motor inhibition and response expectancy: A Laplacian ERP study. *Biological Psychology, 85*, 386–392.
- Meegan, D. V., Aslin, R. N., & Jacobs, R. A. (2000). Motor timing learned without motor training. *Nature Neuroscience, 3*, 860–862.
- Menon, V., Adelman, N. E., White, C. D., Glover, G. H., & Reiss, A. L. (2001). Error-related brain activation during a go/nogo response inhibition task. *Human Brain Mapping, 12*, 131–143.
- Miltner, W. H., Braun, C. H., & Coles, M. G. (1997). Event-related brain potentials following incorrect feedback in a time-estimation task: Evidence for a generic neural system for error detection. *Journal of Cognitive Neuroscience, 9*, 788–798.
- Miyamoto, K., Osada, T., Setsuie, R., Takeda, M., Tamura, K., Adachi, Y., et al. (2017). Causal neural network of metamemory for retrospection in primates. *Science, 355*, 188–193.
- Narayanan, N. S., & Laubach, M. (2006). Top-down control of motor cortex ensembles by dorsomedial prefrontal cortex. *Neuron, 52*, 921–931.
- Nieuwenhuis, S., Ridderinkhof, K. R., Blom, J., Band, G. P., & Kok, A. (2001). Error-related brain potentials are differentially related to awareness of response errors: Evidence from an antisaccade task. *Psychophysiology, 38*, 752–760.
- Palva, S., & Palva, J. M. (2012). Discovering oscillatory interaction networks with M/EEG: Challenges and breakthroughs. *Trends in Cognitive Sciences, 16*, 219–230.
- Praamstra, P., Turgeon, M., Hesse, C. W., Wing, A. M., & Perryer, L. (2003). Neurophysiological correlates of error correction in sensorimotor-synchronization. *Neuroimage, 20*, 1283–1297.
- Rogerson, P. (2001). *Statistical methods for geography*. Los Angeles, CA: Sage.
- Scheffers, M. K., & Coles, M. G. H. (2000). Performance monitoring in a confusing world: Error-related brain activity, judgments of response accuracy, and types of errors. *Journal of Experimental Psychology: Human Perception and Performance, 26*, 141–151.
- Shekhar, M., & Rahnev, D. (2018). Distinguishing the roles of dorsolateral and anterior PFC in visual metacognition. *Journal of Neuroscience, 38*, 5078–5087.
- Simen, P., Balcı, F., de Souza, L., Cohen, J. D., & Holmes, P. (2011). A model of interval timing by neural integration. *Journal of Neuroscience, 31*, 9238–9253.
- Soranzo, A., & Grassi, M. (2014). PSYCHOACOUSTICS: A comprehensive MATLAB toolbox for auditory testing. *Frontiers in Psychology, 5*, 712.
- Taulu, S., & Simola, J. (2006). Spatiotemporal signal space separation method for rejecting nearby interference in MEG measurements. *Physics in Medicine and Biology, 51*, 1759–1768.
- Tremblay, A., & Newman, A. J. (2015). Modeling nonlinear relationships in ERP data using mixed-effects regression with R examples. *Psychophysiology, 52*, 124–139.
- Ullsperger, M., Fischer, A. G., Nigbur, R., & Endrass, T. (2014). Neural mechanisms and temporal dynamics of performance monitoring. *Trends in Cognitive Sciences, 18*, 259–267.
- van Driel, J., Ridderinkhof, K. R., & Cohen, M. X. (2012). Not all errors are alike: Theta and alpha EEG dynamics relate to differences in error-processing dynamics. *Journal of Neuroscience, 32*, 16795–16806.
- van Rij, J., Wieling, M., Baayen, R. H., & van Rijn, H. (2016). Package 'itsadug'. Retrieved from <http://cran.r-project.org/web/packages/itsadug/itsadug.pdf>.
- van Wassenhove, V. (2009). Minding time in an amodal representational space. *Philosophical Transactions of the Royal Society of London, Series B, Biological Sciences, 364*, 1815–1830.
- Whitmarsh, S., Barendregt, H., Schoffelen, J. M., & Jensen, O. (2014). Metacognitive awareness of covert somatosensory attention corresponds to contralateral alpha power. *Neuroimage, 85*, 803–809.

- Wiener, M., Parikh, A., Krakow, A., & Coslett, H. B. (2018). An intrinsic role of beta oscillations in memory for time estimation. *Scientific Reports*, *8*, 7992.
- Wiener, M., Turkeltaub, P., & Coslett, H. B. (2010). The image of time: A voxel-wise meta-analysis. *Neuroimage*, *49*, 1728–1740.
- Wood, S. N. (2003). Thin plate regression splines. *Journal of the Royal Statistical Society of London, Series B (Statistical Methodology)*, *65*, 95–114.
- Wood, S. N. (2009). Package 'mgcv'. Retrieved from <http://cran.r-project.org/web/packages/mgcv/mgcv.pdf>.
- Wood, S. N. (2011). Fast stable restricted maximum likelihood and marginal likelihood estimation of semiparametric generalized linear models. *Journal of the Royal Statistical Society, Series B (Statistical Methodology)*, *73*, 3–36.
- Wood, S. N. (2017). *Generalized additive models: An introduction with R*. Boca Raton, FL: CRC Press.
- Ye, Q., Zou, F., Lau, H., Hu, Y., & Kwok, S. C. (2018). Causal evidence for mnemonic metacognition in human precuneus. *Journal of Neuroscience*, *38*, 6379–6387.
- Yeung, N., Botvinick, M. M., & Cohen, J. D. (2004). The neural basis of error detection: Conflict monitoring and the error-related negativity. *Psychological Review*, *111*, 931–959.
- Zakay, D., & Block, R. A. (1995). An attentional-gate model of prospective time estimation. *Time and the dynamic control of behavior*, 167–178.
- Zatorre, R. J., Chen, J. L., & Penhune, V. B. (2007). When the brain plays music: Auditory–motor interactions in music perception and production. *Nature Reviews Neuroscience*, *8*, 547–558.